DE GRUYTER DOI 10.1515/zpch-2014-0507 — Z. Phys. Chem. 2014; 228(4–5): 351–368

E. Cristina Stanca-Kaposta*, Falko Schwaneberg,
Matias R. Fagiani, Torsten Wende, Franz Hagemann,
Annett Wünschmann, Ludger Wöste, and Knut R. Asmis*

Infrared Photodissociation Spectroscopy of $C_{2n+1}N^-$ Anions with $n = 1–5$

Abstract: The gas phase vibrational spectroscopy of cryogenically cooled $C_{2n+1}N^-$ anions with $n = 1–5$ is investigated in the spectral range of the C≡C and C≡N stretching modes (1850–2400 cm^{-1}) by way of infrared photodissociation (IRPD) spectroscopy of messenger-tagged $C_{2n+1}N^-{\cdot}mD_2$ complexes. The IRPD spectra are assigned based on a comparison to previously reported anharmonic and harmonic CCSD(T) vibrational frequencies and intensities. Experimentally determined and predicted anharmonic vibrational transition energies lie within ±21 cm^{-1}. For the harmonic CCSD(T)/vqz+ vibrational frequencies a scaling factor of 0.9808 is determined, resulting in comparable absolute deviations. The influence of the D_2-messenger molecules on the structure and the IRPD spectrum is found to be small. Compared to the results of previous IR matrix isolation studies additional, in particular weaker, IR-active transitions are identified.

Keywords: Infrared Photodissociation, Messenger Technique, Gas Phase, Ab Initio Calculations, Scaling Factor.

***Corresponding Author: E. Cristina Stanca-Kaposta,** Freie Universität Berlin, Institut für Experimentalphysik, Arnimallee 14, 14195 Berlin, Germany, e-mail: kaposta@physik.fu-berlin.de
Falko Schwaneberg, Franz Hagemann, Annett Wünschmann, Ludger Wöste: Freie Universität Berlin, Institut für Experimentalphysik, Arnimallee 14, 14195 Berlin, Germany
Knut R. Asmis, Fritz-Haber-Institut der Max-Planck-Gesellschaft, Faradayweg 4–6, 14195 Berlin, Germany
Matias R. Fagiani, Torsten Wende: Fritz-Haber-Institut der Max-Planck-Gesellschaft, Faradayweg 4–6, 14195 Berlin, Germany
Torsten Wende: Current address: Physical and Theoretical Chemistry Laboratory, Department of Chemistry, University of Oxford, South Parks Road, Oxford OX1 3QZ, United Kingdom
Knut R. Asmis: Wilhelm-Ostwald-Institut, Universität Leipzig, Linnéstr. 2, D-04103 Leipzig, Germany, e-mail: knut.asmis@uni-leipzig.de

Dedicated to: Professor Klaus Rademann on the occasion of his 60th birthday

1 Introduction

It is well known that dusty circumstellar envelopes are a rich radio source, resulting in the detection of a series of molecules [1–3]. For example, the carbon star IRC +10216 is particularly rich in long linear carbon chains and is the source where the polyacetylenic radicals C_nH (n = 4, 6, 8) [4, 5] and C_nN (n = 3, 5) [6, 7] have been discovered. Beside neutral and cationic molecules, more recently and unexpectedly, molecular anions like C_4H^-, C_6H^- and C_8H^- as well as C_3N^- and C_5N^- have been detected in the interstellar medium and identified by comparison with laboratory experiments [8–12]. Since their discovery in space, these anions have been the subject of intense experimental and theoretical studies and have also motivated this work. Here, we report the gas phase vibrational spectra of cryogenically cooled $C_{2n+1}N^-$ anions with n = 1–5.

Mass spectrometric investigations of laser-ablated cyano-group containing solids and of soot or graphite arcing in a N_2 atmosphere disclosed CN^- and C_3N^- as major products [13]. For C_nN^- clusters an odd/even effect has been observed in which the anions containing an odd number of carbon atoms are more stable, due to their closed electronic shell [13, 14]. Electronic and vibrational absorption spectra of $C_{2n+1}N^-$ (n = 1–4) have mainly been investigated in rare-gas matrices [15–19]. Initial matrix studies on C_3N^- generated via cyanoacetylene dissociation were uncertain regarding the assignment of infrared (IR) absorptions to the anion [16, 17, 20]. Later, more detailed investigations on C_3N^- in different rare-gas matrix environments combined with coupled cluster calculations managed to assign most of the observed IR transitions [18]. The C_5N^- anion has also been investigated by IR matrix-isolation spectroscopy and its IR-active vibrational transitions have been identified based on comparison to density functional theory (DFT) calculations [15]. Experimental as well as theoretical investigations on larger $C_{2n+1}N^-$ anions (n > 2) are scarce. In their matrix studies, which mainly focused on the electronic transitions of $C_{2n+1}N^-$ (n = 2–6) anions, Grutter et al. [19] also reported the IR absorption spectra of the smaller anions and found evidence for a few IR transitions for C_5N^-, C_7N^- and C_9N^-. Garand et al. and Yen et al. [21, 22] investigated the anion photoelectron spectra of the C_nN^- (n = 2–6) clusters using slow electron velocity-map imaging (SEVI) and determined adiabatic electron affinities for C_3N and C_5N, as well as vibrational frequencies for the fundamentals of the degenerate cis (538 cm^{-1}) and trans (208 cm^{-1}) bending modes of C_3N^-. The observation of little vibrational activity upon photodetachment of the anions with an even number of carbon atoms and the detection of transitions to the neutral quartet state indicated that the investigated $C_{2n}N^-$ anions have all linear geometries and $^3\Sigma^-$ ground states.

The C_nN^- anions, especially C_3N^- and C_5N^-, have been the subject of a series of theoretical studies [18, 23–26]. Zhan and Iwata, using second-order Møller-Plesset (MP2) perturbation theory, predicted singlet ground states for C_2N^-, C_4N^- and C_6N^- of which the last two exhibited non-linear geometries [25, 27]. Subsequent DFT studies, however, contested these predictions, finding linear geometries for all investigated C_nN^- anions with singlet $^1\Sigma^+$ and triplet $^3\Sigma^-$ ground states for the anions with odd and even number of carbon atoms, respectively [23]. The latter results are supported by the SEVI experiments of Garand et al. and Yen et al. [21, 22]. Botschwina et al. performed a detailed theoretical analysis of the $C_{2n+1}N^-$ ($n = 1–6$) anions using coupled cluster theory combined with large basis sets and predicted, among other spectroscopic constants, their equilibrium structures as well as harmonic ($n = 1–6$) and anharmonic ($n = 1–3$) vibrational frequencies [18, 24]. All investigated anions exhibit linear equilibrium geometries and singlet $^1\Sigma^+$ ground states, in agreement with the DFT calculations of Pascoli and Lavendy [23].

We use gas phase infrared photodissociation (IRPD) spectroscopy to characterize the vibrational transitions of $C_{2n+1}N^-$ anions with $n = 1–5$ in the spectral region of the C≡C and C≡N stretching modes. The vibrational action spectra are measured by monitoring the IR-photoinduced loss of D_2-messenger molecules from $C_{2n+1}N^-{\cdot}mD_2$ complexes as a function of the photon energy. The IRPD spectra are assigned on the basis of a comparison to previously calculated vibrational frequencies from coupled cluster theory [18, 24].

2 Experimental and computational details

IRPD experiments were performed on an ion-trap tandem mass-spectrometer, described in detail elsewhere [28, 29]. Briefly, $C_nN_m^-$ anions are produced by reactive sputtering of a graphite target (Kurt J. Lesker) within a magnetron sputter source [30]. Ar- and N_2-gas are used for the reactive sputtering process which leads to formation of C_nN_m clusters in different charge states. Cluster aggregation occurs in a He-atmosphere (6.0, Linde AG). The beam of anions passes a skimmer held at variable potential and is collimated in a He-filled radio-frequency (RF) decapole ion-guide. The ions of interest are mass-selected in a quadrupole mass-filter (Extrel CMS), deflected into 90° by an electrostatic quadrupole ion-deflector and focused into a linear ring-electrode RF ion-trap. The trap is filled with pure D_2 buffer gas and held at 15–20 K using a closed-cycle He cryostat in order to avoid condensation of the D_2 gas. Trapped ions are vibrationally cooled by collisions with the buffer gas close to the ambient temperature. At sufficiently low ion-

trap temperatures the formation of ion-messenger complexes, i.e. $C_nN^-{\cdot}mD_2$, via three-body collisions is observed [31, 32]. After the trap is filled for 99 ms all ions are extracted from the trap and focused both temporarily and spatially into the center of the extraction region of a time-of-flight (TOF) mass-spectrometer, where they are irradiated by a tunable wavelength IR laser pulse.

IR excitation is performed using pulsed laser radiation in the 1850–2400 cm^{-1} range. The radiation between 1850–2140 cm^{-1} is produced by an OPO/OPA/$AgGaSe_2$ IR laser system (LaserVision) [33], pumped by a seeded Nd:YAG laser (Continuum, Powerlite DLS-8000). The pump laser operates at 10 Hz and provides 7 ns long pulses. The pulse energies were ≤3 mJ and were further attenuated, when necessary, to avoid saturation. For IR radiation between 2050–2400 cm^{-1}, a second OPO/OPA system (LaserVision), pumped by a pulsed Nd:YAG laser (Innolas, Spitlight 600), is used. Typical pulse energies are ≤2 mJ. The IR laser pulses enter the vacuum chamber through a KBr window. IRPD spectra are recorded by monitoring all ion intensities simultaneously as the photon wavelength is scanned. The photodissociation cross section σ is determined from the relative abundances of the parent and photofragment ions, $I_p(\nu)$ and $I_f(\nu)$, respectively, and the frequency-dependent laser fluence (assuming a constant interaction volume throughout the range of scanned wavelengths) $\varphi(\nu)$ according to [34]:

$$\sigma = -\ln[I_p(\nu)/(I_p + I_f)]/\varphi(\nu) \quad (1)$$

The number of attached D_2 molecules depends on the trapping conditions, the temperature of the trap as well as the nature of the parent ion. For the best signal-to-noise ratio trapping conditions are chosen such that the highest intensity of the tagged-complex is achieved, leading typically from one to up to three D_2 molecules per complex. IRPD spectra are generated by summing over the photodepletion signals from all D_2 complexes.

Electronic structure calculations using the coupled cluster method including single and double excitations (CCSD) [35, 36] and the Dunning's correlation-consistent aug-cc-pVTZ [37–39] (avtz) basis set are performed using the Gaussian 09 program package [40]. The previously reported structures of the bare anions [24] serve as input for our geometry optimizations. To account for anharmonic effects as well as systematic errors on the harmonic force constants, a scaling factor is determined for the harmonic frequencies by comparing the experimental IRPD bands of $C_{2n+1}N^-{\cdot}mD_2$ (n = 2–5, m = 1–4) with the ones predicted for the pure anions. Optimal scaling factors (λ) are determined by a least-square proce-

dure, minimizing the residual γ [41]:

$$\gamma = \sum_{i=1}^{n} (\omega_i^{\exp} - \lambda\omega_i^{\text{theor}})^2 \quad (2)$$

Where n is the total number of modes for all anions and ω_i^{exp} and ω_i^{theor} are the i^{th} experimental fundamental frequency and the i^{th} theoretical harmonic frequency (in cm^{-1}), respectively. The optimized scaling factor is used to determine an overall root-mean-square, rms [41]:

$$\text{rms} = \left(\sum_{1}^{n} \gamma/n \right)^{1/2} \quad (3)$$

The dissociation energy of $C_3N^-\cdot D_2$ is calculated at the same level of theory and is corrected for the basis set superposition error using the counterpoise correction of Boys and Bernardi [42]. Rotational band profiles are simulated using the rotational constant B obtained from our calculations on $C_3N^-\cdot D_2$ (B = 2500.59 MHz, D_2 attached to the C-site) and assuming a change of the rotational constant in the excited vibrational state of 0.5% (ν_2 mode) and 1% (ν_1 mode) [43, 44] as inputs for the PGopher software [45]. The spectra are convoluted using a Gaussian line shape function with FWHM of 4.5 cm^{-1} to account for the laser bandwidth (~2.5 cm^{-1}) as well as other effects.

3 Results and discussions

Figure 1 shows a typical mass spectrum of $C_nN_m^-$ cluster anions ($1 \le n \le 12$, $0 \le m \le 5$) obtained by reactive sputtering of a graphite target with a 1 : 3 Ar/N_2 gas mixture. Binary cluster anions with a maximum of four N atoms are predominantly generated. As reported previously, C_nN^- and $C_nN_3^-$ clusters exhibit an odd/even effect [13, 14, 46]. While C_nN^- clusters with an odd n are more stable and thus more abundant than those with an even n, the situation is reversed for $C_nN_3^-$ clusters, where those with even n are more abundant.

3.1 IRPD spectra of $C_{2n+1}N^-\cdot mD_2$ complexes

The D_2-predissociation spectra of $C_{2n+1}N^-\cdot mD_2$ ($1 \le n \le 5$, $1 \le m \le 3$) complexes from 1850 to 2400 cm^{-1} are shown in Figure 2. The spectra are spliced together from individual scans over the two emission ranges of the IR lasers. As these emission ranges overlap by almost 100 cm^{-1} the presence of absorption bands

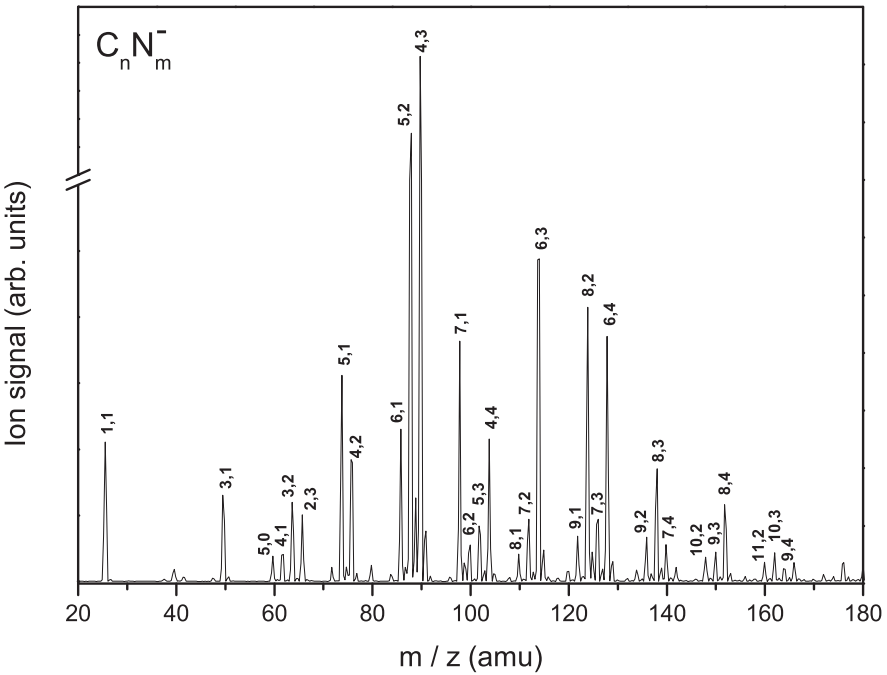

Figure 1: Quadrupole mass-spectrum of anions obtained by reactive sputtering of a graphite target with Ar/N_2 gas. The mass peaks of $C_nN_m^-$ clusters are marked by (n, m).

in this region aids in the determination of the relative peak intensities as the spectra are combined. This is the case for all systems studied here except for $C_3N^- \cdot mD_2$. In this case the relative intensities were obtained using Equation (1). Figure 2 compares the experimental spectra with the previously reported CCSD(T) anharmonic (for $n = 1-3$) and scaled harmonic (for $n = 4, 5$) vibrational frequencies [18, 24]. Table 1 lists the IRPD band positions, the CCSD(T) anharmonic and scaled harmonic frequencies, the vibrational transitions obtained from matrix-IR measurements as well as the experimental and calculated relative intensities. The harmonic frequencies for the larger $C_{2n+1}N^-$ ($n = 2-5$) anions are scaled by 0.9808 (see computational details). The root-mean-square error obtained from Equation (3) is 11 cm^{-1}.

The IRPD spectrum of $C_3N^- \cdot mD_2$ with $m = 1-2$ (see Figure 2a), measured between 1850–2400 cm^{-1}, shows two main features centered at 1952 and 2180 cm^{-1} with an intensity ratio of 1 : 4. The number, position and intensity order of the experimental bands is reproduced by the CCSD(T)/avqz calculations and hence the two observed vibrational transitions are assigned accordingly, i.e. to the fun-

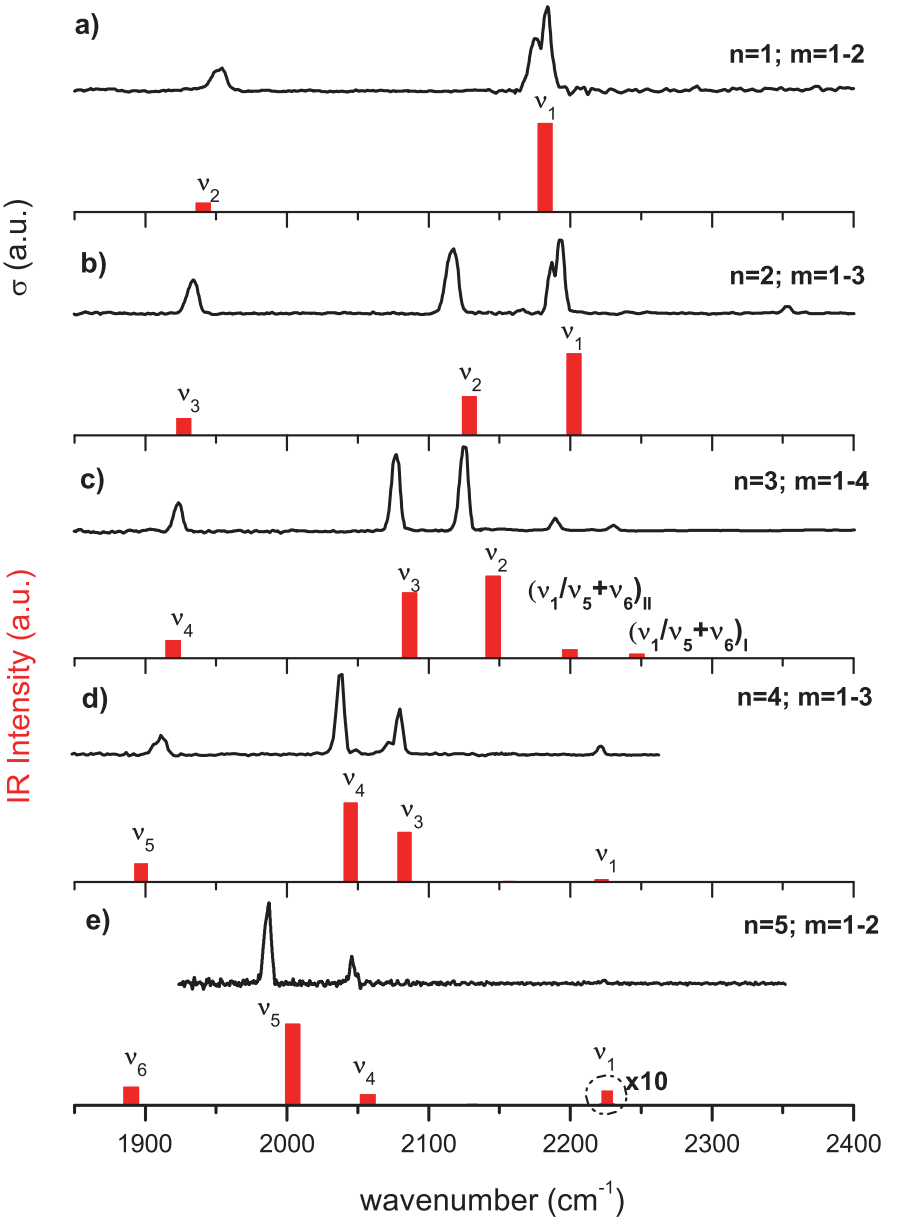

Figure 2: The experimental IRPD spectra (black traces) of $C_{2n+1}N^-{\cdot}mD_2$ ($1 \le n \le 5$, $1 \le m \le 4$) compared to CCSD(T) anharmonic ($n = 1-3$) and scaled harmonic ($n = 4, 5$) frequencies (solid red bars) of $C_{2n+1}N^-$ anions. [18, 24] For $n = 5$ the intensity of the predicted ν_1 mode has been enhanced by a factor of 10 for a better visibility.

Table 1: Experimental IRPD (gas phase) and matrix-IR band positions as well as calculated anharmonic and scaled harmonic vibrational frequencies (in cm^{-1}) for $C_{2n+1}N^-$ ($n = 1–5$). The IR intensities are given as percent relative to the strongest band. For the IRPD peaks, the band centers are given. The differences between anharmonic, respectively scaled harmonic and gas phase frequencies are given in square brackets.

	Mode	IRPD	Matrix IR			CCSD(T)/avqz[d] CCSD(T)/vqz+	
			Ar	Ne	Kr	scaled harmonic[e]	anharmonic
C_3N^-	ν_1	2180 (100)	2178.7[a] (52)	2178[a]	2173.9[a] (73)		2182.3 [+2] (100)
			2173.0[a] (100)	2176[a]	2168.8[a] (100)		
	ν_2	1952 (25)	1944.3[a] (14)		1940.3[a] (16)		1940.9 [−11] (10)
C_5N^-		2353 (10)					
	ν_1	2191 (100)	2183.8[b] (100)			2193 [+2]	2202.6 [+12] (100)
	ν_2	2116 (88)	2111.3[b] (83)	2115.9[c]		2114 [−2]	2128.6 [+13] (47)
	ν_3	1934 (45)	1923.2[b] (83)			1914 [−20]	1927.2 [−7] (21)
	ν_4					1156	1167.7
C_7N^-	$(\nu_1/\nu_5+\nu_6)_I$	2230 (6)				2210* (14)	2247 [+17] (5)
	$(\nu_1/\nu_5+\nu_6)_{II}$	2190 (15)					2199.7 [+10] (10)
	ν_2	2125 (100)		2123.8[c]		2131 [+6] (100)	2145.6 [+21] (100)
	ν_3	2077 (90)		2073.7[c]		2073 [−4] (74)	2086.5 [+10] (80)
	ν_4	1923 (33)				1905 [−18] (20)	1919.5 [−3] (21)
C_9N^-	ν_1	2221 (12)				2222 [+1] (3)	
	ν_2					2157 (1)	
	ν_3	2079 (57)				2083 [+4] (63)	

Table 1: Continued.

	Mode	IRPD	Matrix IR			CCSD(T)/avqz[d] CCSD(T)/vqz+	
			Ar	Ne	Kr	scaled harmonic[e]	anharmonic
		2072 (17)					
		2048 (7)					
	ν_4	2037 (100)		2033.2[c]		2045 [+8] (100)	
	ν_5	1909 (25)				1897 [−12] (23)	
$C_{11}N^-$	ν_1	2224 (4)				2226 [+2] (2)	
	ν_2					2172 (~0)	
	ν_3					2131 (~0)	
	ν_4	2046 (34)				2057 [+11] (13)	
	ν_5	1986 (100)				2004 [+18] (100)	

[a] Ar-, Ne- and Kr-Matrix IR transitions from Ref. [18].
[b] Ar-matrix (Ref. [15])
[c] Ne-matrix (Ref. [19])
[d] CCSD(T)/avtz for C_3N^- (Ref. [18]) and CCSD(T)/vqz+ for the other $C_{2n+1}N^-$ anions (Ref. [24]).
[e] Scaling factor for the $C_{2n+1}N^-$ anions: 0.9808 for $n = 2–5$.
[*] ν_1 vibrational mode of C_7N^-.

damentals of the pseudosymmetric (ν_1) and pseudoantisymmetric (ν_2) combinations of the C-C and C-N triple bond stretching local modes.

Figure 2b compares the IRPD spectrum of $C_5N^-{\cdot}mD_2$ ($m = 1–3$) in the spectral range from 1850 to 2400 cm^{-1} to anharmonic CCSD(T)/vqz+ vibrational frequencies and intensities [24]. Four main features are observed in the IRPD spectrum at 2353, 2191, 2116 and 1934 cm^{-1}, of which the central two are the most intense (see Table 1). The calculations on the bare C_5N^- predict only three bands within our scanning range, two with a higher intensity centered at 2203 cm^{-1}, 2129 cm^{-1} and a weaker one at 1927 cm^{-1} with an intensity ratio of 5 : 2 : 1. Their positions are within 13 cm^{-1} of the corresponding experimental band, and

we therefore assign the three IRPD peaks below 2200 cm^{-1} to the ν_1, ν_2 and ν_3 stretching modes, respectively. The weak feature at 2353 cm^{-1} is not predicted by the harmonic calculations.

The IRPD spectrum of $C_7N^-{\cdot}mD_2$ ($m = 1-4$) is shown together with the CCSD(T)/vqz+ anharmonic frequencies and intensities [24] in Figure 2c. Five peaks are observed in the IRPD spectrum. In the order of decreasing intensity these are found at 2125, 2077, 1923, 2190 and 2230 cm^{-1}. The anharmonic calculations also predict five vibrational frequencies in this range (Table 1) with the same intensity ordering. The two highest energy bands are thus assigned to a Fermi-type resonance between the fundamental of the ν_1 mode and the $\nu_5 + \nu_6$ combination band, followed by the ν_2, ν_3 and ν_4 modes at lower energies. The calculated anharmonic frequencies lie within 21 cm^{-1} of the experimental bands. The scaled harmonic calculations show a similar agreement with experiment (± 18 cm^{-1}), but cannot reproduce the doublet at higher energies, as it originates from an anharmonic effect.

The gas phase IRPD spectrum of $C_9N^-{\cdot}mD_2$ ($m = 1-3$) between 1850 to 2300 cm^{-1} is shown together with the CCSD(T) /vqz+ scaled harmonic frequencies and intensities in Figure 2d. Four peaks are observed at 2221, 2079, 2037 and 1909 cm^{-1} and correspond to the fundamentals of the ν_1, ν_3, ν_4 and ν_5 modes, calculated within ± 12 cm^{-1} of the experimental counterpart at 2222, 2083, 2045 and 1897 cm^{-1}, respectively. The experimentally observed relative intensities are qualitatively reproduced (see Table 1). A fifth transition is predicted at 2157 cm^{-1} (ν_2), which is not observed in the IRPD spectrum. However, this transition is predicted to be very weak (44 km/mol), explaining why it is not resolved in the experimental spectrum in Figure 2d.

The largest anion investigated in this study is $C_{11}N^-{\cdot}mD_2$ ($m = 1-2$). Its gas phase IRPD spectrum in the range from 1920 to 2300 cm^{-1} is shown in Figure 2e together with the predicted scaled harmonic frequencies and intensities (see also Table 1). The IRPD spectrum reveals three bands at 2224, 2046 and 1986 cm^{-1}, of which the lowest energy one is the most intense. The calculations predict three harmonic frequencies (Table 1) with significant intensity in the investigated range. These are the fundamental transitions exciting the ν_1 (2226 cm^{-1}), ν_4 (2057 cm^{-1}) and ν_5 (2004 cm^{-1}) stretching modes, whose relative intensities qualitatively match the experimental observation. The ν_2 (2172 cm^{-1}) and ν_3 (2131 cm^{-1}) modes are not predicted to be substantially IR active and are also not resolved in our IRPD spectra.

3.2 Band contours

Additional structure in the form of asymmetric band shapes is observed in the IRPD spectra of the smallest two C_nN^- anions shown in Figure 2. For C_3N^- two maxima are resolved for the ν_1 (2177 and 2182 cm^{-1}) and ν_2 (1948 and 1953 cm^{-1}) bands, reminiscent of rotational structure. The full-width-half-maximum of the two bands (~12 cm^{-1}) are considerably larger than the laser bandwidth and hence we attribute them to the P and R branches of transitions involving rotationally-excited linear $C_3N^-{\cdot}D_2$ anions. Simulated rotational profiles, shown in Figure 3, reproduce this structure satisfactorily. The best agreement is obtained assuming a Boltzmann distribution with a mean rotational temperature of 75 K. This value is considerably higher than the trap temperature (15 K), but similar to previously obtained rotational temperatures for other systems [47, 48]. The apparent elevated rotational temperature is probably the result of a combination of effects, including (a) RF heating, (b) rotational excitation upon extraction of the ions from the gas-filled ion trap, (c) anions entering the trap at the end of the trapping cycle, which did not undergo sufficient collisions to completely thermalize, and (d) a non-Boltzmann-like distribution of the rotational energy [34].

For C_5N^- the asymmetric band profile, including the relative intensities of the two maxima for the ν_1 band, is very similar to that observed for C_3N^- and we attribute it to the same effect. The ν_2 and ν_3 bands of C_5N^- also show considerable broadening due to rotational excitation, but the individual rotational branches are not as well resolved. For the larger clusters no rotational structure is resolved anymore, since the rotational constants decrease as the length of the carbon chain increases.

3.3 The influence of the messenger molecules

In order to investigate, to what extent the D_2-messenger molecules perturb the geometric structure and the associated vibrational frequencies, we determined CCSD/avtz equilibrium bond lengths and harmonic vibrational frequencies of bare C_3N^- as well as the N- and C-site $C_3N^-{\cdot}D_2$ complexes (see Tables 2 and 3). The global minimum-energy structure of bare C_3N^-, as well as those of larger $C_{2n+1}N^-$ clusters ($^1\Sigma^+$ ground states), [24] is linear and N-terminated [18, 22]. For the messenger-tagged C_3N^- anion, D_2 binds collinear to either the terminal C-atom (C-site) or N-atom (N-site). The C-site complex is preferred by ~1 kJ/mol. Complexation to D_2 leaves the C_3N^- bond lengths (<0.01 Å, see Table 2) and vibrational frequencies (≤2 cm^{-1} for the stretching modes, see Table 3) nearly unchanged. Hence, the perturbation of the IR spectrum is predicted to be small and

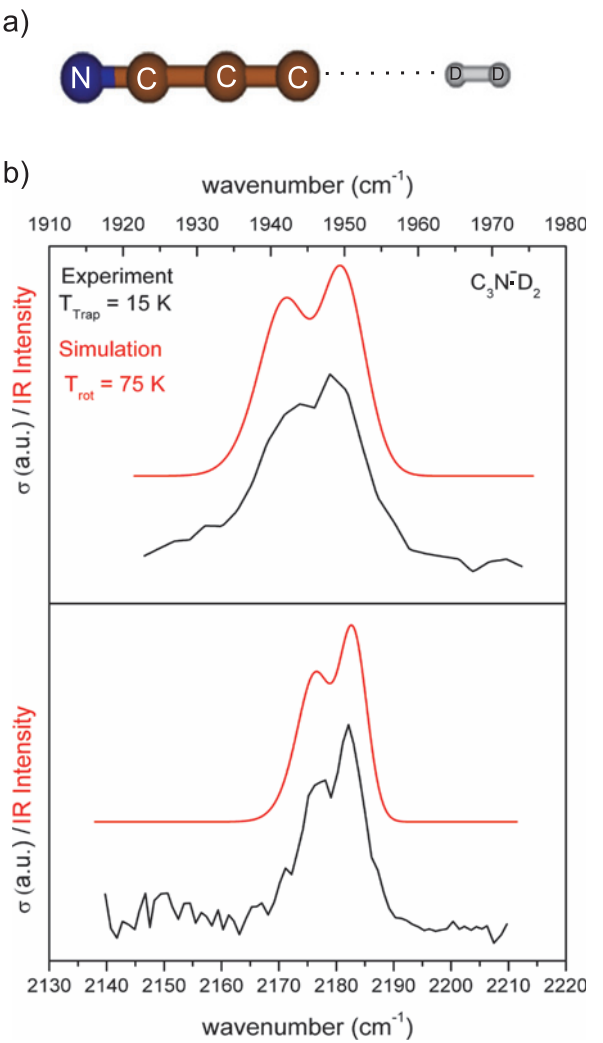

Figure 3: (a) Minimum-energy structure used for the band profile analysis. (b) Comparison of the IRPD spectra of $C_3N^-{\cdot}mD_2$ to simulated rotational band profiles (red traces). See text for details of the simulation.

on the order of the laser pulse bandwidths. Complex formation is predicted to lead to a substantial red-shift of the D_2 vibrational frequency. Interestingly, the red-shift induced by binding to the C-site ($-87\ cm^{-1}$) is nearly twice as large as for the N-site ($-49\ cm^{-1}$), while the C$\cdots$D bond (2.74 Å) is predicted slightly longer

Table 2: Equilibrium bond lengths (in Å) for C_3N^-, D_2 and the N- and C-site $C_3N^-{\cdot}D_2$ complexes.

C_3N^- species	Method	$r(C_1C_2)$	$r(C_2C_3)$	$r(C_3N)$	r(ND)	r(CD)	r(DD)
C_3N^-	CCSD(T)/acv5z*#	1.252	1.366	1.171			
	CCSD/avtz*	1.249	1.376	1.171			
$C_3N^-{\cdot}D_2$ (N-site)	CCSD/avtz*	1.249	1.375	1.167	2.597		0.747
$C_3N^-{\cdot}D_2$ (C-site)	CCSD/avtz*	1.248	1.376	1.167		2.739	0.750
Free D_2	CCSD/avtz*						0.743
	CCSD(T)/avqz*p						0.741

* acv5z – aug-cc-pCV5Z basis set; avtz – aug-cc-pVTZ basis set; avqz - aug-cc-pVQZ basis set
# Empirically corrected values. From Ref. [18].
p From Ref. [49].

Table 3: Experimental gas phase and harmonic vibrational frequencies (in cm^{-1}) for C_3N^- and $C_3N^-{\cdot}D_2$.

C_3N-species	Method	ν_{D-D}	ν_1	ν_2	ν_3	ν_4	ν_a*	ν_5	ν_b*	ν_c*
C_3N^-	CCSD/avtz		2291	2027	882	542		201		
$C_3N^-{\cdot}D_2$ (N-site)	CCSD/avtz	3064	2293	2029	884	544	351	205	129.5	18
$C_3N^-{\cdot}D_2$ (C-site)	CCSD/avtz	3026	2292	2027	885	544	307	201.5	132	25
Free D_2	CCSD/avtz	3113								

* ν_a – N$\cdots$D-D bending motion, ν_b – N$\cdots$D, respectively C$\cdots$D stretch, ν_c – C≡N$\cdots$D bending vibration.

then the N$\cdots$D bond (2.60 Å) length, effects which result from the negative charge localized at the terminal C-atom.

Finally, we also calculated the dissociation energies (D_2-loss) of the C-site and N-site complexes. The predicted dissociation energies (D_0) for the D_2-loss channel are smaller than 350 cm^{-1}, i.e. they are smaller than the photon energies used in the present study, suggesting that the absorption of a single photon is sufficient to break the anion-D_2 bond.

All anion-D_2 complexes probed here contain more than a single D_2 molecule, due to experimental reasons. Complexes containing a single D_2 molecule are most abundant (usually by a factor of seven or more relative to two D_2 ligands) and hence the IRPD spectra should mainly reflect the photodissociation cross section of the singly-tagged species. However, since the dipole moments of the anions in-

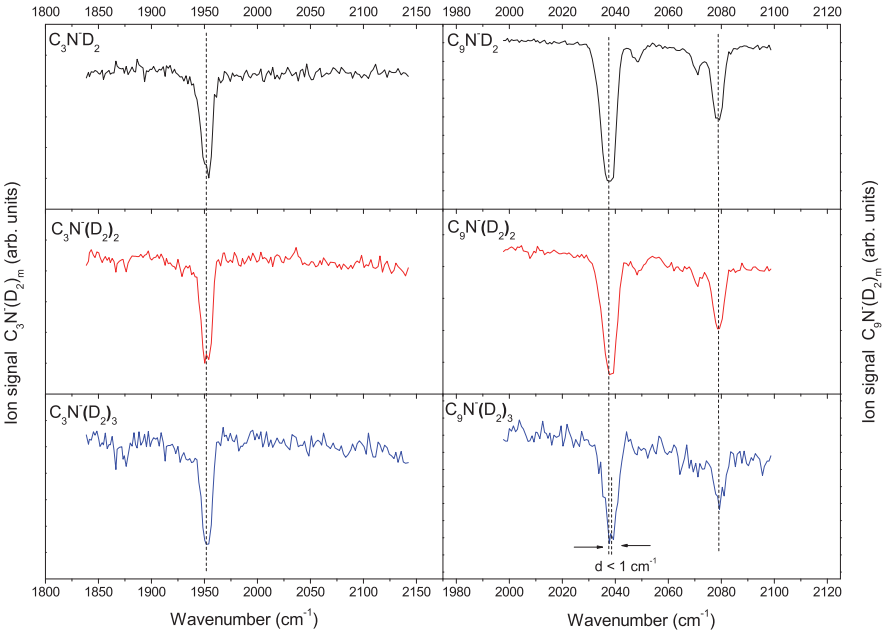

Figure 4: Comparison of the ion yields of the product mass channels corresponding to $C_3N^-{\cdot}mD_2$ (left) and $C_9N^-{\cdot}mD_2$ (right) with $m = 1–3$.

crease substantially with chain length [24], the interaction with D_2 and thus its influence on the IRPD spectrum is stronger for the longer chain anions. We checked for such effects by comparing the ion yields of the product mass channels corresponding to $C_{2n+1}N^-$ anions tagged with one, two and three D_2 ligands. Figure 4 shows an example for $C_3N^-{\cdot}mD_2$ and $C_9N^-{\cdot}mD_2$ ($m = 1–3$). The detected shifts are less than 1 cm^{-1}, again indicating a negligible perturbation of the IRPD spectrum.

3.4 Comparison to IR matrix isolation results

With the exception of $C_{11}N^-$ the anions investigated here have previously been studied by direct IR absorption spectroscopy of matrix-isolated species. The frequencies of the detected vibrational transitions, which were attributed to C_nN^- anions, are listed in Table 1. In general, a reasonable agreement is observed between the matrix IR and the gas phase IRPD data. The gas phase to matrix red shifts Δ_{g-m} of less than −12 cm^{-1} are within the expected range for the stretching

vibrations [50, 51]. Some differences, however, are observed. The matrix studies on C_3N^- found three IR transitions corresponding to the anion, one more than detected in the gas phase. Two of these, located at 2178.7 and 1944.3 cm^{-1} in the Ar-matrix (their equivalent values are 2173.9 and 1940.3 cm^{-1} in Kr-matrix and 2176 cm^{-1} in Ne-matrix) match our assignment based on the present gas phase values of 2180 cm^{-1} (ν_1) and 1952 cm^{-1} (ν_2) .

The third IR transition, observed at 2173, 2168.8 and 2176 cm^{-1} in Ar-, Kr- and Ne-matrix, respectively, was tentatively attributed to a matrix-mediated higher-order resonance between the fundamental frequency of the stretching vibration ν_1 and the third overtone of the cis bending mode ν_4 ($v_4 = 4$) [18]. No such transition is observed in our gas phase spectra, confirming its matrix-mediated nature. Furthermore, our results also support the conclusion of Kołos et al. [18, 20] that the absorption observed by Guennoun et al. [16] at 2194 cm^{-1} cannot be attributed to the C_3N^- anion.

Good agreement is also found between the Ar-matrix isolation studies of Coupeaud et al. [15] on C_5N^-, who identified the ν_1, ν_2 and ν_3 stretching vibrations at 2183.8, 2111.3 and 1923.2 cm^{-1}, respectively. The fourth transition observed at 2355 cm^{-1} in the present study, was not reported, possibly due to its low IR intensity. In a similar study of mass-selected $C_{2n+1}N^-$ ($n = 2–4$) deposited in solid Ne. [19] Grutter et al. were able to detect only a limited number of IR-transitions for these anions, namely at 2115 cm^{-1} (ν_2) for C_5N^-, at 2123.8 (ν_2) and 2073.7 cm^{-1} (ν_3) for C_7N^- and at 2033.2 cm^{-1} (ν_4) for C_9N^- (see Table 1). The position of these bands are very close to the gas phase values, with gas to matrix shifts of less than -4 cm^{-1}.

4 Summary and conclusions

The IRPD spectra of $C_{2n+1}N^-{\cdot}mD_2$ ($n = 1–5$, $m = 1–4$), measured in the C-C and C-N triple bond stretching region, are reported and assigned based on a comparison to CCSD(T) vibrational frequencies. An absolute deviation between experimental and predicted anharmonic CCSD(T)/vqz+ frequencies of 21 cm^{-1} or less is found and the predicted intensity ordering of the individual IR active transitions is confirmed. A scaling factor of 0.9808 is determined for harmonic CCSD(T)/vqz+ frequencies, yielding frequencies with comparable deviations to those from the anharmonic calculations. Comparison to the results from previous IR matrix isolation studies allows us to determine a gas phase to matrix shift for the stretching vibrations of $\Delta_{g-m} \leq -12$ cm^{-1}. Moreover, the present gas phase IRPD spectra allow the identification of additional, in particular weaker, IR active transitions.

These results of the present study should prove beneficial in future attempts to detect these species in the interstellar medium as well as in predicting the IR spectra of related compounds.

Acknowledgement: The authors express their greatest thanks to Prof. Dr. Klaus Rademann (Berlin) for the support of the project, in which this technique was developed, at the beginnings of the Dedicated Research Center SFB 546 of the German Research Foundation and to Prof. Dr. John Maier (Basel), Alexander von Humbold fellow at the Freie Universität Berlin, for helpful and stimulating discussions.

Received January 17, 2014; accepted April 08, 2014.

References

1. J. Cernicharo, M. Guélin, and C. Kahane, Astron. Astrophys. Suppl. Ser. **142** (2000) 181.
2. K. Kawaguchi, M. Ohishi, S. Ishikawa, and N. Kaifu, Astrophys. J. **386** (1992) L51.
3. S. Green, Ann. Rev. Phys. Chem. **32** (1981) 103.
4. J. Cernicharo and M. Guélin, Astron. Astrophys. **309** (1996) L27.
5. M. Guélin, S. Green, and P. Thaddeus, Astrophys. J. **224** (1978) L27.
6. M. Guélin and P. Thaddeus, Astrophys. J. **212** (1977) L81.
7. M. Guélin, N. Neininger, and J. Cernicharo, Astron. Astrophys. **335** (1998) L1.
8. J. Cernicharo, M. Guélin, M. Agúndez, M. C. McCarthy, and P. Thaddeus, Astrophys. J. **688** (2008) L83.
9. P. Thaddeus, C. A. Gottlieb, H. Gupta, S. Brünken, M. C. McCarthy, M. Agúndez, M. Guélin, and J. Cernicharo, Astrophys. J. **677** (2008) 1132.
10. J. Cernicharo, M. Guélin, M. Agúndez, K. Kawaguchi, M. McCarthy, and P. Thaddeus, Astron. Astrophys. **467** (2007) L37.
11. M. C. McCarthy, C. A. Gottlieb, H. Gupta, and P. Thaddeus, Astrophys. J. **652** (2006) L141.
12. S. Brünken, H. Gupta, C. A. Gottlieb, M. C. McCarthy, and P. Thaddeus, Astrophys. J. **664** (2007) L43.
13. C. Wang, R. Huang, Z. Liu, and L. Zheng, Chem. Phys. Lett. **237** (1995) 463.
14. Z. Tang, R. Huang, L. Shi, and L. Zheng, Int. J. Mass. Spec. Ion Proc. **173** (1998) 71.
15. A. Coupeaud, M. Turowski, M. Gronowski, N. Piétri, T. Couturier-Tamburelli, R. Kołos, and J.-P. Aycard, J. Chem. Phys. **128** (2008) 154303.
16. Z. Guennoun, I. Couturier-Tamburelli, N. Piétri, and J. P. Aycard, Chem. Phys. Lett. **368** (2003) 574.
17. L. Khriachtchev, A. Lignell, H. Tanskanen, J. Lundell, H. Kiljunen, and M. Räsänen, J. Phys. Chem. A **110** (2006) 11876.
18. R. Kołos, M. Gronowski, and P. Botschwina, J. Chem. Phys. **128** (2008) 154305.
19. M. Grutter, M. Wyss, and J. P. Maier, J. Chem. Phys. **110** (1999) 1492.

20. R. Kołos, *Carbon-Nitrogen Chain Molecules in the Laboratory and in Interstellar Medium*, Institute of Physical Chemistry of the Polish Academy of Sciences Warsaw, (2003).
21. E. Garand, T. I. Yacovitch, and D. M. Neumark, J. Chem. Phys. **130** (2009) 064304.
22. T. A. Yen, E. Garand, A. T. Shreve, and D. M. Neumark, J. Phys. Chem. A **114** (2010) 3215.
23. G. Pascoli and H. Lavendy, Chem. Phys. Lett. **312** (1999) 333.
24. P. Botschwina and R. Oswald, J. Chem. Phys. **129** (2008) 044305.
25. C. Zhan and S. Iwata, J. Chem. Phys. **104** (1996) 9058.
26. M. M. Al Mogren, A. A. El-Azhary, W. Z. Alkiali, and M. Hochlaf, J. Phys. Chem. A **114** (2010) 12258.
27. C.-G. Zhan and S. Iwata, J. Chem. Phys. **105** (1996) 6578.
28. D. J. Goebbert, G. Meijer, and K. R. Asmis, AIP Conf. Proc. **1104** (2009) 22.
29. D. J. Goebbert, E. Garand, T. Wende, R. Bergmann, G. Meijer, K. R. Asmis, and D. M. Neumark, J. Phys. Chem. A (R. Gerber Festschrift) **113** (2009) 7584.
30. H. Haberland, M. Karrais, and M. Mall, Z. Phys. D **20** (1991) 413.
31. M. Brümmer, C. Kaposta, G. Santambrogio, and K. R. Asmis, J. Chem. Phys. **119** (2003) 12700.
32. D. J. Goebbert, T. Wende, R. Bergmann, G. Meijer, and K. R. Asmis, J. Phys. Chem. A **113** (2008) 5874.
33. W. R. Bosenberg and D. R. Guyer, J. Opt. Soc. Am. B **10** (1993) 1716.
34. T. Wende, *Gas Phase Infrared Photodissociation Spectroscopy of Mass-Selected Ionic Clusters: Metal Oxides and Microhydrated Anions*, PhD Thesis, Freie Universität Berlin, Berlin (2012).
35. G. D. Purvis III and R. J. Bartlett, J. Chem. Phys. **76** (1982) 1910.
36. G. E. Scuseria, C. L. Janssen, and H. F. Schaefer III, J. Chem. Phys. **89** (1988) 7382.
37. T. H. Dunning Jr., J. Chem. Phys. **90** (1989) 1007.
38. R. A. Kendall, T. H. Dunning Jr., and R. J. Harrison, J. Chem. Phys. **96** (1992) 6796.
39. D. E. Woon and T. H. Dunning Jr., J. Chem. Phys. **98** (1993) 1358.
40. M. J. Frisch, G. W. Trucks, H. B. Schlegel, G. E. Scuseria, M. A. Robb, J. R. Cheeseman, G. Scalmani, V. Barone, B. Mennucci, G. A. Petersson, H. Nakatsuji, M. Caricato, X. Li, H. P. Hratchian, A. F. Izmaylov, J. Bloino, G. Zheng, J. L. Sonnenberg, M. Hada, M. Ehara, K. Toyota, R. Fukuda, J. Hasegawa, M. Ishida, T. Nakajima, Y. Honda, O. Kitao, H. Nakai, T. Vreven, J. A. Montgomery Jr., J. E. Peralta, F. Ogliaro, M. Bearpark, J. J. Heyd, E. Brothers, K. N. Kudin, V. N. Staroverov, R. Kobayashi, J. Normand, K. Raghavachari, A. Rendell, J. C. Burant, S. S. Iyengar, J. Tomasi, M. Cossi, N. Rega, J. M. Millam, M. Klene, J. E. Knox, J. B. Cross, V. Bakken, C. Adamo, J. Jaramillo, R. Gomperts, R. E. Stratmann, O. Yazyev, A. J. Austin, R. Cammi, C. Pomelli, J. W. Ochterski, R. L. Martin, K. Morokuma, V. G. Zakrzewski, G. A. Voth, P. Salvador, J. J. Dannenberg, S. Dapprich, A. D. Daniels, Ö. Farkas, J. B. Foresman, J. V. Ortiz, J. Cioslowski, and D. J. Fox, Gaussian 09, Revision A02, Gaussian, Inc., Wallingford, CT (2009).
41. J. P. Merrick, D. Moran, and K. Radom, J. Phys. Chem. A **111** (2007) 11683.
42. S. F. Boys and F. Bernardi, Mol. Phys. **19** (1970) 553.
43. H-S. Andrei, N. Solcà, and O. Dopfer, Angew. Chem. Int. Ed. **47** (2008) 395.
44. A. Van Orden and R. J. Saykally, Chem. Rev. **98** (1998) 2313.
45. C. M. Western, PGOPHER, a Program for Simulating Rotational Structure, University of Bristol, http://pgopher.chm.bris.ac.uk.
46. A. K. Gupta and P. Ayyub, Eur. Phys. J. D **17** (2001) 221.

47. A. M. Burow, M. Sierka, R. Wlodarczyk, J. Sauer, T. Wende, P. Claes, L. Jiang, G. Meijer, P. Lievens, and K. R. Asmis, Phys. Chem. Chem. Phys. **13** (2011) 19393.
48. D. J. Goebbert, G. Meijer, and K. R. Asmis, AIP Conf. Proc. **1104** (2009) 22.
49. B. L. Poad, V. Dryza, J. Klos, A. A. Buchachenko, and E. J. Bieske, J. Chem. Phys. **134** (2011) 214302.
50. A. D. Abbate and C. B. Moore, J. Chem. Phys. **82** (1985) 1255.
51. F. Stroh, B. P. Winnewisser, M. Winnewisser, H. P. Reisenauer, G. Maier, S. J. Goede, and F. Bickelhaupt, Chem. Phys. Lett. **160** (1989) 105.